JGR Oceans

RESEARCH ARTICLE
10.1029/2020JC016523

Distribution and Transport of Water Masses in the East Siberian Sea and Their Impacts on the Arctic Halocline

Xiaoyu Wang[1,2], Jinping Zhao[1,2], Vyacheslav B. Lobanov[3], Dmitry Kaplunenko[3], Yan N. Rudykh[3], Yan He[4], and Xianyao Chen[1,2]

[1]Frontier Science Center for Deep Ocean Multispheres and Earth System (FDOMES) and Physical Oceanography Laboratory, Ocean University of China, Qingdao, China, [2]Laboratory for Ocean Dynamics and Climate, Qingdao Pilot National Laboratory for Marine Science and Technology, Qingdao, China, [3]V.I. Il'ichev Pacific Oceanological Institute, Far Eastern Branch Russian Academy of Sciences, Vladivostok, Russia, [4]The First Institute of Oceanography, Qingdao, China

Key Points:

- Fresh and salty East Siberian shelf waters are identified using in situ hydrographic observations
- Up to three types of halocline waters in the Makarov Basin originate in the East Siberian Sea (ESS)
- An eastward transport of shelf waters across the ESS is strengthened by cyclonic Arctic circulation

Correspondence to:
X. Wang,
wangxiaoyu331@163.com

Citation:
Wang, X., Zhao, J., Lobanov, V. B., Kaplunenko, D., Rudykh, Y. N., He, Y., & Chen, X. (2021). Distribution and transport of water masses in the East Siberian Sea and their impacts on the Arctic halocline. *Journal of Geophysical Research: Oceans*, *126*, e2020JC016523. https://doi.org/10.1029/2020JC016523

Received 18 JUN 2020
Accepted 15 JUL 2021

Abstract We investigated the transport of Arctic shelf water and its impacts on the downstream hydrographic structures in the Amerasian Basin by combining data collected in the summer of 2016 from two international cruises in the Pacific sector. The East Siberian Sea (ESS), in which cold shelf water with salinity of 31.0–32.8 is produced, was identified to be a major source of the near-freezing temperature water for the Makarov Basin. This relatively low-salinity shelf water was transported into the Chukchi Abyssal Plain and occupied the subsurface layer (30–60 m), which led to the formation of a subsurface oceanic front stretching along the Chukchi Plateau and northern side of the Mendeleev Ridge. The offshore transport of waters from the ESS caused an intrusion of the Atlantic Water onto the shelf and promoted the formation of the diapycnally mixed Lower Halocline Water (D-LHW) at the bottom of the outer shelf. Our findings indicate that the source of the D-LHW in the Arctic Pacific sector might extend from the Chukchi Plateau to as far as the Makarov Basin. We hypothesize that advection of waters from the ESS into the Makarov Basin promotes development of the subsurface halocline in the Makarov Basin. The volume transport of surface waters (salinity less than 30) on the ESS shelf was estimated to be about 0.6 Sv (10^6 m^3 s^{-1}) eastward to the Canada Basin in 2016, consistent with the cyclonic Arctic circulation regime in 2016.

Plain Language Summary The East Siberian Sea (ESS) is an important freshwater reservoir of the Arctic Ocean, but the water transport across the ESS remains poorly understood because there are few observations. In 2016, two hydrographic cruises were conducted in the ESS and nearby basins to reveal how water masses in the ESS affects ocean temperature and salinity downstream. We found that the ESS is the source of up to three different water masses that are found in the adjacent Makarov Basin. These water masses occupy a total thickness of about 100 m in the water column. We found that low-salinity waters on the shelf of the ESS flowed toward the Chukchi Abyssal Plain, carrying a large amount of freshwater from the continental shelf of Russia into the Makarov Basin. We estimated that the volume of freshwater provided by the ESS is similar to the flow through the Bering Strait, indicating an important role of the ESS in the Arctic freshwater budget.

1. Introduction

The East Siberian Sea (ESS; Figure 1) covers an area of 9.36×10^5 km^2 (Timokhov, 1994). Its average depth is about 54 m, its maximum depth is 915 m, and its total volume is about 49,000 km^3 (Timokhov, 1994). The positive buoyancy input provided by river discharge drives an eastward-flowing low-salinity current called the Siberian Coastal Current (Chapman & Lentz, 1994; Münchow et al., 1999). The direction and along-coast extent of the coastal current are also influenced by surface wind stress, which determines the freshwater transport along the continental shelf of Russia (Osadchiev et al., 2020; Savel'eva et al., 2008; Weingartner et al., 1999).

The main factors affecting the properties of water masses in the ESS include river runoff, sea ice melting and refreezing, solar radiation, and inputs of the Atlantic-origin and Pacific-origin waters. In summer, a warm and fresh surface mixed layer of ~20–30 m thick is formed on the shelf; this is called the mixed

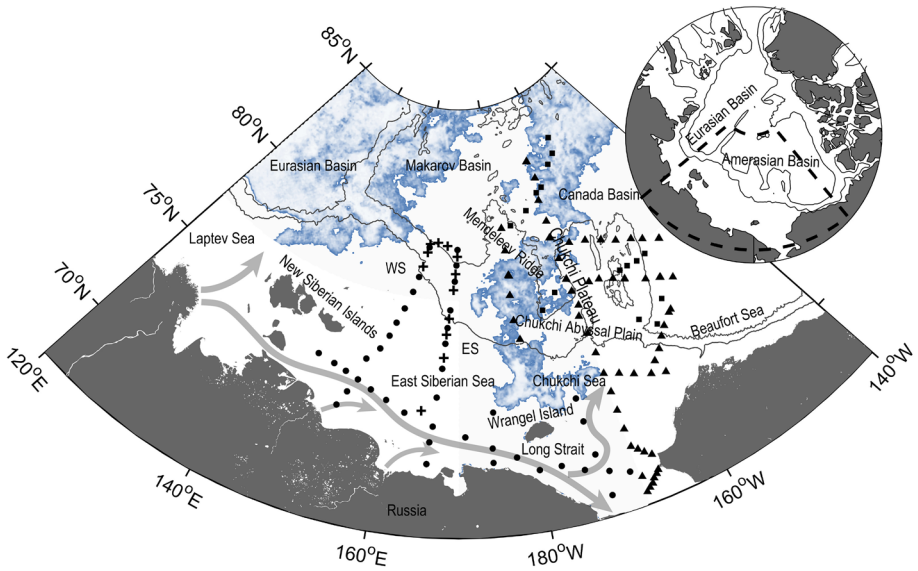

Figure 1. Locations of hydrographic stations in the summer of 2016. Black dots and crosses denote the Conductivity, Temperature, Depth (CTD) and XCTD stations of the Russia cruise (La-77); black triangles and squares denote the CTD and XCTD stations of the China cruise (CHINARE-7). Eastern section and western section stands for the western and eastern meridional hydrographic sections, respectively. Black contours denote 200- and 2,000-m isobaths; steel blue shadow denotes the sea ice extent on September 8, 2016. Gray arrows denote the Siberian Coastal Current from Weingartner et al. (1999).

layer water (MLW) (Baumann et al., 2018; Jackson et al., 2010; Morison et al., 1998). The MLW is mainly composed of meltwater and river runoff, leading to wide variations in temperature and salinity (Carmack et al., 2016; Polyakov et al., 2018). In winter, vertical mixing on the ESS shelf is strengthened by the cooling and brine injection from ice growth, resulting in a well-mixed layer with the temperature decreasing nearly to the freezing point (<−1.5°C) from surface to bottom (Bauch et al., 2012; Jones & Anderson, 1986). Even in the following summer, the remnant winter water beneath the thermocline can still maintain its original features of near-freezing temperature, low potential vorticity and relatively high salinity (Bauch et al., 2005; Gong & Pickart, 2016; Pickart et al., 2005).

Under the mixed layer in the Makarov Basin, there is an Arctic halocline layer about 100–200 m thick, with strong stratification and temperature below −1.0°C (Figure 2b). Waters in the Arctic halocline can be divided into three subtypes according to different salinity (S) ranges that are the results of different sources or formation processes. From shallow to deep waters, these layers are: transitional halocline water (THW, $29.5 < S < 32.8$), upper halocline water (UHW, $32.8 < S < 34.0$), and lower halocline water (LHW, $S > 34.0$) (Anderson, et al., 2013; Bauch et al., 2014; Morison et al., 1998; Shimada et al., 2001). The THW, which has the same salinity range as the summer Bering Sea Water but is colder, mainly lies beneath the mixed layer as the shallowest part of the halocline (Morison et al., 1998). The UHW is formed by advective processes from the Arctic shelf (Anderson et al., 2017; Jones & Anderson, 1986; Steele & Boyd, 1998). Note that in the Canada Basin there also exists a part of the halocline called the UHW (Shimada et al., 2005), which originates from winter modification of the Pacific-origin water in the Chukchi Sea. In general, the UHW in the Makarov Basin is much more stratified than that in the Canada Basin.

The LHW is formed in the Barents Sea and Nansen Basin by winter modification of the Atlantic Water and is characterized by a sharp bend in the θ-S curve at salinity range of 34.0–34.5 (Figure 2c) (Alkire et al., 2017; Kikuchi et al., 2004; Rudels et al., 2004). In addition, a relatively warm halocline water type, which is called diapycnally mixed LHW (D-LHW), can be formed by the mixing of the Atlantic Water and shelf water along the Chukchi and Beaufort slopes (Itoh et al., 2007; Woodgate et al., 2005). The formation of the D-LHW is related to the upwelling of the Atlantic Water from the continental slope to the shelf, which is a response to the regionally wind-induced surface Ekman transport (Lin et al., 2019; Meneghello et al., 2018; Nikolopoulos et al., 2009; Pickart et al., 2011).

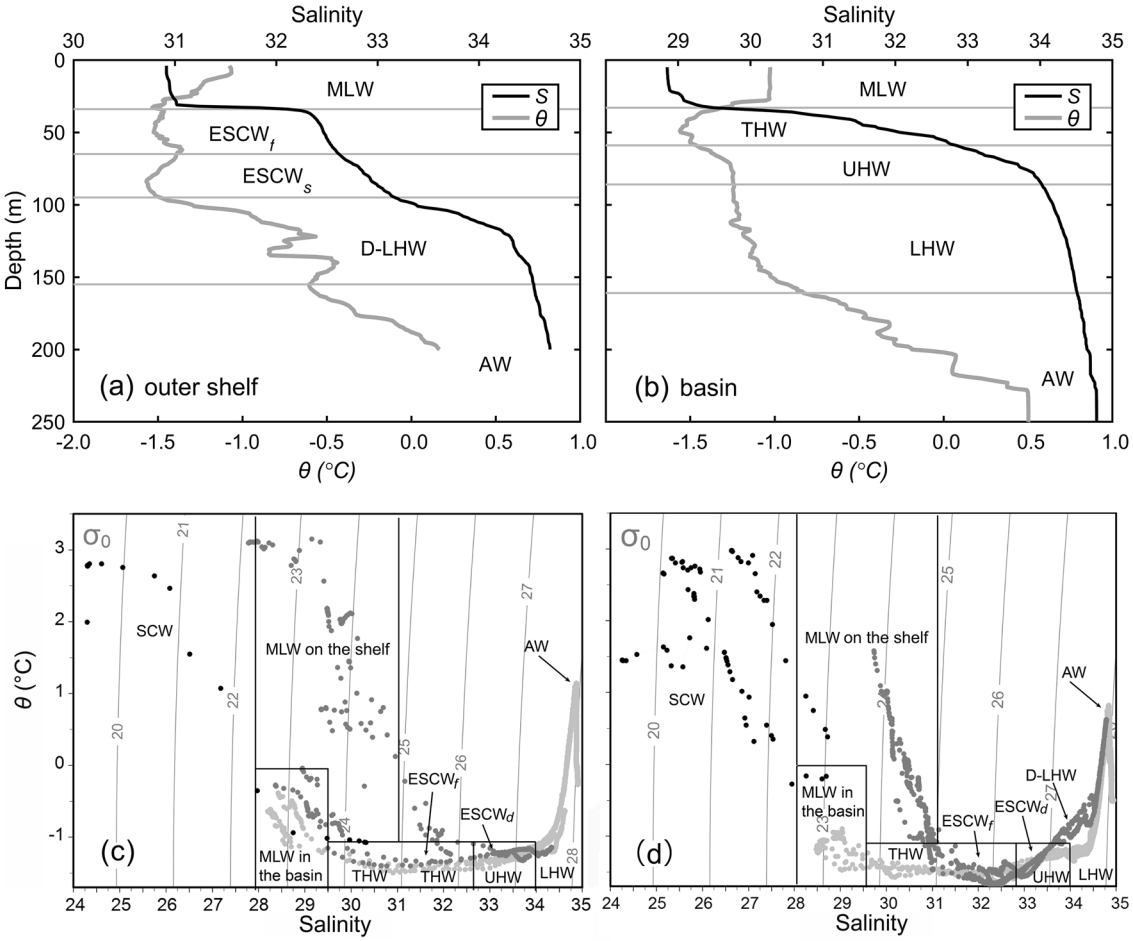

Figure 2. (a) and (b) show the typical θ (gray line) and S (black line) profiles, with water masses labeled, on the outer shelf and in the southern Makarov basin, respectively. (c) and (d) show the θ-S diagrams in western section and eastern section, respectively. The major water masses are delineated by the black lines. Light gray, gray, and dark gray colors used for dots denote θ and S profiles collected from different stations (corresponding to colored triangles in Figures 3a and 3b).

The upper Arctic Ocean is strongly influenced by the transport and modification of water masses from the ESS (Aksenov et al., 2011). First, the transport direction of shelf waters reflects the state of the transpolar drift in the Arctic Ocean. An eastward transport of shelf waters generally indicates that the axis of the Transpolar Drift Current changes from the Eurasian Basin toward the side of the Canada Basin (Bauch et al., 2011; Dmitrenko et al., 2005; Morison et al., 2012; Steele et al., 2004). Accompanied by the axis moving eastward, the cold halocline layer in the Eurasian Basin begins to weaken or even disappear completely (Johnson & Polyakov, 2001; Schlosser et al., 2002; Steele & Boyd, 1998). If the axis of the transpolar drift turns back along the Lomonosov Ridge, the cold halocline appears to recover in the Eurasian Basin (Björk et al., 2002; Boyd et al., 2002). Second, the ESS is currently an important source for the Arctic halocline water. Early studies suggested that waters in the ESS provided little input to the halocline due to the low salinity and large cover of sea ice (Aagaard et al., 1981; Chapman & Lentz, 1994). However, the salinity of shelf waters has increased in recent decades (Dmitrenko et al., 2008; Williams & Carmack, 2015), and parts of the waters close to the slope are now dense enough to supply the Arctic halocline in the Makarov Basin (Alkire et al., 2019; Anderson et al., 2013; Bauch et al., 2016). Anderson et al. (2017) confirmed that the region around the New Siberian Islands could produce a kind of halocline water with salinity higher than 33.0. In addition, a relatively fresh and cold shelf water ($32 < S < 32.5$, $\theta < -1.5$°C) was observed in the western Chukchi Sea (Kawaguchi et al., 2015; Linders et al., 2017; McLaughlin et al., 1996; Zhao et al., 2015). This water mass is also hypothesized to originate in the ESS (Jones et al., 2008; McLaughlin et al., 2004; Nishino et al., 2008, 2013).

Based on these previous studies, we expect the wide shelf of the ESS will contain various water masses with large differences in properties. However, the distribution and transport of these waters are still not fully understood. In this study, we used hydrographic data collected during the joint Russia-China cruise (La-77 cruise), which was conducted by *R/V Akademik M.A. Lavrentiev* from 19 August to 20 September in 2016, to explore the transport of shelf water in the ESS. We also used hydrographic data collected by *R/V Xuelong* over the same period. The structure of the paper is as follows. We describe the hydrographic data in Section 2. In Section 3, we classify and present all the existing water masses across the shelf in the ESS. In Section 4, we focus on the distribution and transport of shelf waters from the shelf to the Amerasian Basin. In Section 5, we investigate the relationship between shelf water transport and the formation of the halocline in the Amerasian Basin. We summarize our main conclusions and discuss their significance in Section 6.

2. Hydrographic Data

The sea ice in the Arctic Pacific Sector between 150°E and 170°E retreated to a record low in September 2016 (Figure 1). During this period, two oceanographic expeditions were conducted simultaneously in the ESS and around the Chukchi Plateau.

The first expedition was carried out by Russian vessel *R/V Akademik M.A. Lavrentyev* in the ESS and Chukchi Sea from 24 August to 16 September, with hydrographic profiles made along two sections extending across the shelf into the Makarov Basin, and one section along the coastline (Figure 1). A total of 57 temperature-salinity profiles were collected. Of these, 45 profiles were obtained using an SBE-911 plus Conductivity, Temperature, Depth (CTD) sensor with temperature and salinity accuracies of 0.001°C and 0.003, respectively, and 12 profiles were obtained using expendable CTD (XCTD) profilers with temperature and salinity accuracies of 0.02°C and 0.04, respectively. The CTD casts were calibrated and processed according to standard Sea-Bird processing procedures.

The second expedition was carried out by the Chinese icebreaker *R/V Xuelong* in the Chukchi Plateau during the same period. A total 72 temperature-salinity profiles were collected to the north of the Bering Strait using the same type of instrument as on the Russian expedition, that is, the SBE-911 plus CTD sensor. The temperature and salinity accuracies are also 0.001°C and 0.003, respectively.

We used daily sea-level pressure (SLP) and 10-m winds from the ECMWF reanalysis product (ERA-5), which has a 0.25° × 0.25° grid spacing (Hersbach et al., 2018). Sea ice velocities were obtained from the Polar Pathfinder daily 25-km EASE-grid sea ice motion vectors (Tschudi et al., 2019), provided by the National Snow and Ice Data Center of the United States (available at https://nsidc.org/data/nsidc-0116). Surface absolute geostrophic velocities were derived from absolute dynamic topography, which is a multi-mission altimeter product from the Copernicus Marine Environment Monitoring Service (https://marine.copernicus.eu/).

3. Water Masses in the East Siberian Sea and Makarov Basin

Temperature and salinity transects for the two meridional sections, the western section (WS) and the eastern section (ES), with locations shown in Figure 1, are given in Figure 3. Following previous studies (Anderson, et al., 2017; Morison et al., 1998; Steele & Boyd, 1998; Woodgate et al., 2005), we define four distinct water masses to study the hydrographic properties in this area, including the mixed layer water (MLW), East Siberian cold shelf water (ESCW), Arctic halocline waters, and Atlantic Water (AW). We further categorize these water masses into several subtypes (Table 1).

3.1. Mixed Layer Water (MLW)

Figures 3c and 3d show a remarkable salinity difference (up to 3.0) between the Siberian Coastal Water (SCW) and MLW on the mid-shelf, which formed oceanic fronts at 73.5°N in section ES and at 74.0°N in section WS, respectively. We found that the front extended nearly along the 30-m isobath (Figure 4a), suggesting a west-to-east water transport of the SCW along the coast. In the western Chukchi Sea (180°–170°W), only a small amount of the SCW was found, with slightly modified salinity ($28.0 < S < 30.0$).

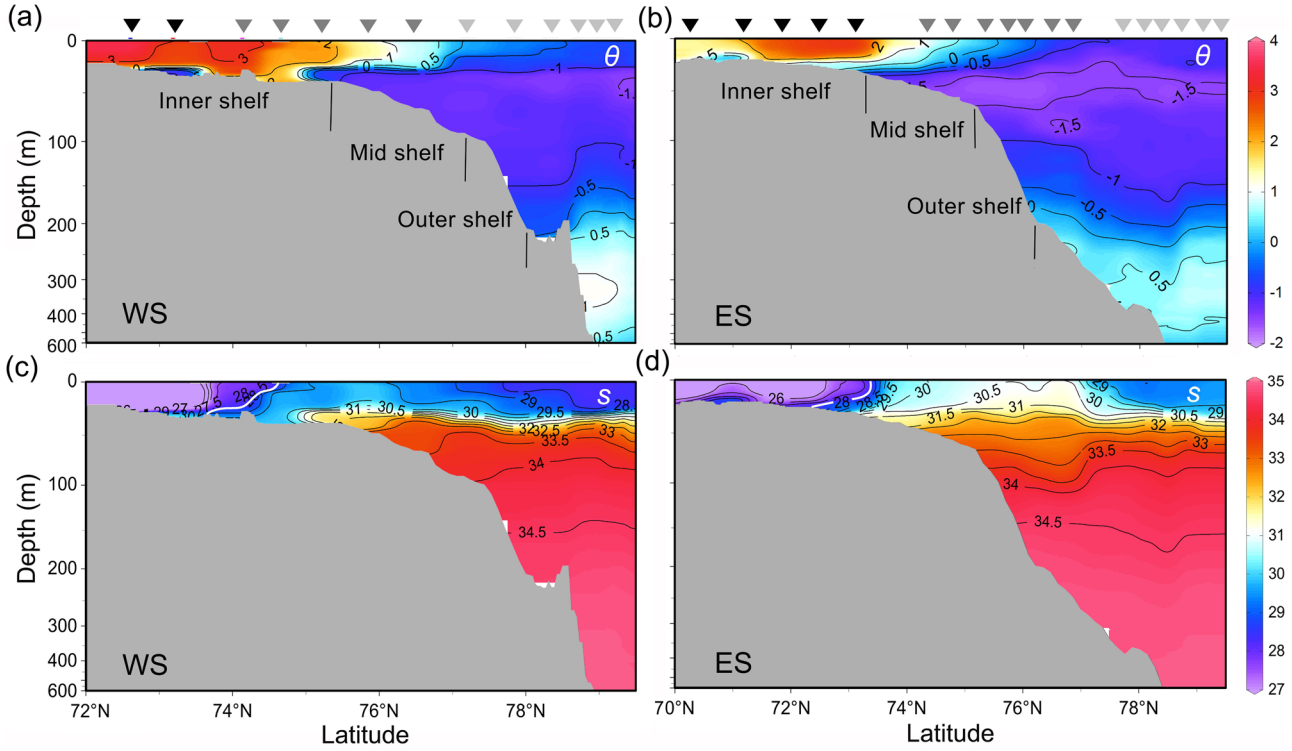

Figure 3. (a) and (b) show the potential temperature along the eastern section (ES) and western section (WS), respectively; black, gray, and light gray triangles denote the station locations in Figures 2c and 2d. (c) and (d) show the salinity along the ES and WS, respectively. The bold white contours denote the salinity value of 28.0. Note that the exponential coordinate is used for the *y*-axis to highlight the hydrographic structure in the upper layer.

At the same time, the freshwater tongue of the SCW extended from the estuarine area toward the northeastern ESS, suggesting an offshore transport of the SCW via the outer shelf to the north of Wrangel Island rather than to the Long Strait in September 2016. This is consistent with the surface current in the ESS derived from the absolute dynamic height during the period of the expedition (24 August to 16 September) (Figure 4c). The axis of the eastward flow, with the maximum speed exceeding 15 cm/s, was found along the isohalines between 26.0 and 28.0, while the eastward component of the flow in the Long Strait (180°) was only about 2–3 cm/s, almost an order of magnitude smaller than the flow across the section ES (~168°E).

Table 1
Water Mass Classification in the ESS

Water mass	Subtype	θ (°C)	Salinity	Absolute salinity (g/kg)	Depth (m)
Mixed Layer Water (MLW)	Siberian Coastal Water (SCW)	1.0–4.0	<28.0	<28.13	0–25
	MLW in the basin	−1.5–0.0	28.0–29.5	28.13–29.64	0–25
	MLW on the shelf	−1.0–3.0	28.0–31.0	28.13–31.15	0–45
East Siberian Cold Shelf Water (ESCW)	Fresh ESCW ($ESCW_f$)	−1.7–0.7	31.0–32.8	31.15–32.96	15–65
	Salty ESCW ($ESCW_s$)	−1.7–1.2	32.8–34.0	32.96–34.16	40–100
Arctic Halocline Waters	Transitional Halocline Water (THW)	−1.70–1.40	29.5–32.8	29.64–32.96	20–65
	Upper Halocline Water (UHW)	−1.65–1.20	32.8–34.0	32.96–34.16	40–100
	Lower Halocline Water (LHW)	−1.35–1.15	34.0–34.5	34.16–34.66	50–150
	Diapycnally mixed Lower Halocline Water (D-LHW)	−1.15–0.50	33.6–34.5	33.76–34.66	80–150
Atlantic Water (AW)	only the top half of AW	−0.50–1.16	34.60–34.87	34.77–35.04	150–350

Abbreviation: ESS, East Siberian Sea.

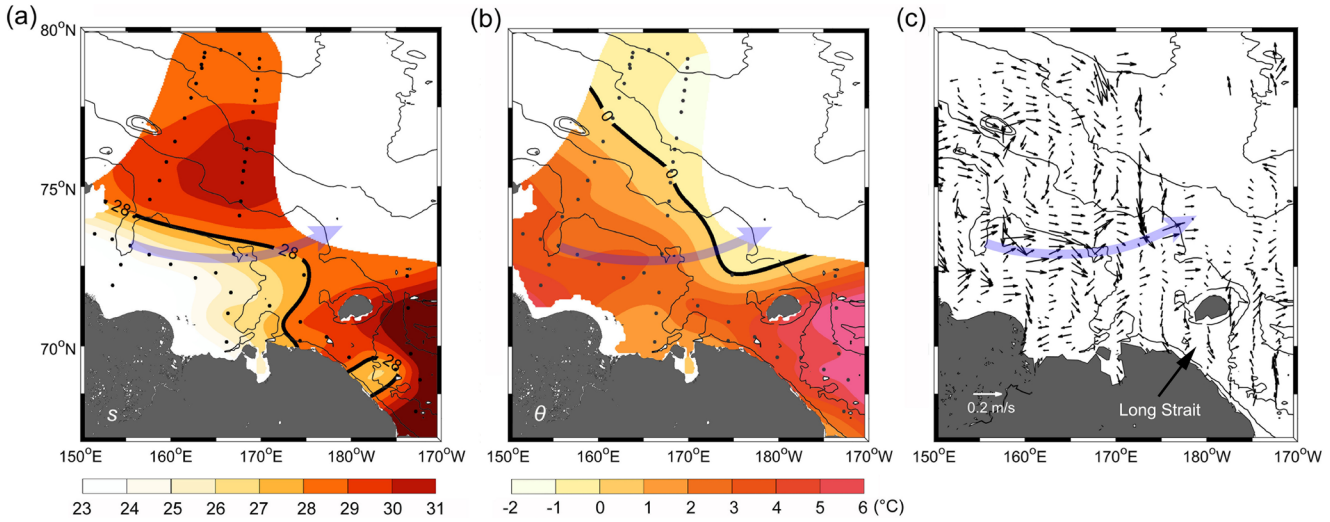

Figure 4. Distribution of (a) salinity and (b) temperature of the Mixed Layer Water. (c) Mean surface velocities derived from the absolute dynamic height. Blue arrow denotes the overall transport of surface waters.

From the coast to the shelf edge (200-m depth) along 168°E, the volume flux of the surface-layer water with a mean thickness of 30 m was estimated to be 0.6 Sv (1 Sv = 10^6 m^3/s). Taking the mean depth of the ESS (~54 m) into account, the total volume flux from the ESS toward the Chukchi Plateau might reach the same level as that via the Bering Strait. More importantly, during our survey the waters on the shelf of the ESS were much fresher than those in the Pacific inflow, thereby making a more important contribution to the freshwater content in the Amerasian Basin.

3.2. East Siberian Cold Shelf Water (ESCW)

Although the MLW warms up during the summer, the waters beneath the MLW can still maintain the low temperature ($\theta < -1$°C) gained during convection in winter (Figures 2a, 3a and 3b); therefore, it is called cold shelf water or remnant winter water (Gong & Pickart, 2016; Okkonen et al., 2019). In the summer of 2016, the East Siberian cold shelf water (ESCW) was found on the mid and outer shelves, occupying a layer in the depth range about 40–100 m (Figure 5). The salinity of the ESCW varied significantly between sections ES and WS, with the salinity range of 32.5–34.0 in section WS and 31.0–33.5 in section ES (Figures 3c and 3d).

In these two regions, the water temperatures are nearly same, but their salinity differences (about 1.0–1.5) cause significant density differences in the ESCW. Once the ESCW is transported into the deep basin, ESCW with different densities will enter different isopycnal layers. To track their transformations, we separate the

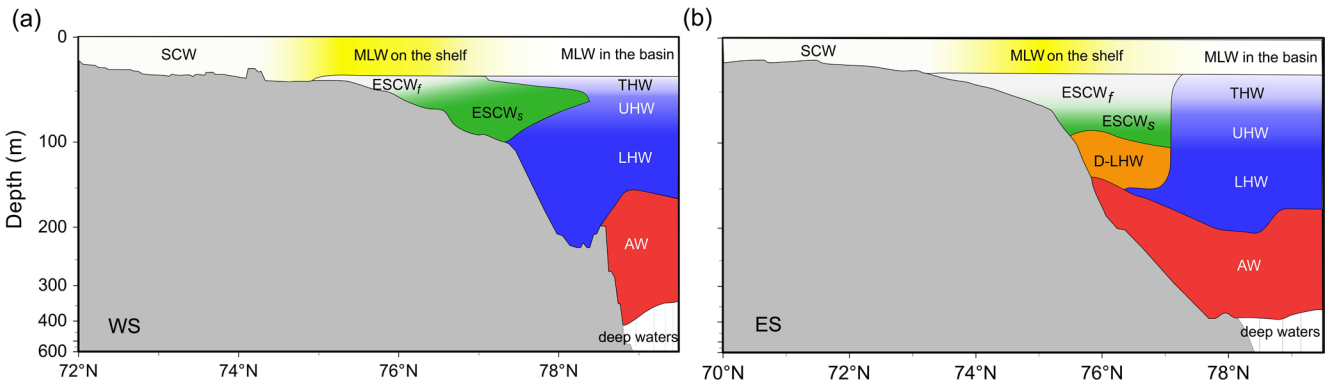

Figure 5. Water masses along (a) western section and (b) eastern section.

ESCW into different water mass sub-types. We use the salinity 32.8 as a criterion to classify the ESCW into two sub-types: fresh ESCW ($ESCW_f$, $S < 32.8$) and salty ESCW ($ESCW_s$, $S > 32.8$). We chose a threshold of $S = 32.8$ because the salinity of the summer Bering Sea water is generally less than 32.8 (Gong & Pickart, 2016; Morison et al., 1998), while the winter Bering Sea water and UHW are larger than 32.8 (Shroyer & Pickart, 2018; Steele et al., 2004; Woodgate et al., 2005). With this separation, the source of the $ESCW_s$ is found mainly in the western ESS close to the outer shelf where the supply of Atlantic-origin water is sufficient in winter (Alkire et al., 2019; Anderson et al., 2013, 2017). In this study, we mainly focus on the formation and distribution of $ESCW_f$.

3.3. Atlantic Water (AW)

In the section WS, the maximum temperature of the AW was about 1.10°C, while in the section ES located 150 km downstream, the maximum temperature decreased to about 0.83°C (Figures 2c and 2d). If we assume the mean velocity of the AW along the slope is 0.05 m/s (Woodgate et al., 2005), the maximum upward heat flux from the core of the AW to the halocline (~200 m depth) would be about 60 W/m^2. We propose that this significant heat flux is related to vigorous tidal mixing between the upwelled AW and the cold waters above the continental slope (Rippeth et al., 2015).

3.4. Arctic Halocline Water

Three halocline water types, discriminated by their salinities, were observed on the slope and in the Makarov Basin during the expeditions. From shallow to deep waters, we can see the THW ($29.5 < S < 32.8$), UHW ($32.8 < S < 34.0$) and LHW ($34.0 < S < 34.5$) in Figure 5. The LHW was slightly modified with about 0.5°C warming after entering the ESS from the Eurasian Basin due to the upward mixing of the Atlantic Water along its transport path (Dmitrenko et al., 2011; Rudels, 2015). The D-LHW was found on the bottom of the outer shelf and slope. Its vertical structure in θ and S are shown in Figure 2.

4. Distribution and Transport of ESCW

4.1. Distribution of ESCW in the ESS

It is difficult to distinguish the cold shelf water and halocline water on the θ-S diagrams (Figures 2c and 2d) due to their similar temperature-salinity relationship with temperature near freezing point and salinity less than 34.0. Nishino et al. (2008) suggest using the potential vorticity (PV) to distinguish these two water masses because the cold shelf water generally showed a low PV due to cooling-driven convection in winter. In this study, the PV was calculated using the method in Katsura (2018). Briefly, when applying the hydrostatic approximation and ignoring the relative vorticity, the PV is simplified as $gf\frac{\partial \sigma_\theta}{\partial p}$, where g is the gravity constant, f is the Coriolis parameter, p is pressure, and σ_θ is potential density.

In the stations XCTD01, LA22, and XCTD03 along the section ES (Figure 6a), the cold shelf waters with salinity between 31.0 and 32.8 all showed a minimum PV lower than 2.0×10^{-9} m^{-1} s^{-1} (Figures 6b and 6c). These widely spread waters were $ESCW_f$, as described in Section 3.2. In contrast, in stations LA25, LA27, and LA28, the water with the same salinity range showed a much higher PV and was only distributed on the slope and further north. These waters were THW.

Bottom hydrographic conditions between sections WS and ES were distinctly different. The dominant bottom water mass in section WS was the $ESCW_s$ ($32.8 < S < 34.0$), with only a small volume of $ESCW_f$ ($31.0 < S < 32.8$) in the shallow mid-shelf less than 50-m depth (Figure 7a). However, in section ES, the $ESCW_f$ became dominant with a horizontal extent of nearly 400 km, from the mid-shelf (~73°N) to the slope (~77°N) (Figure 7b), while the $ESCW_s$ lay beneath the $ESCW_f$ with higher PV and smaller thickness than in the section WS, suggesting an advection of water from section WS.

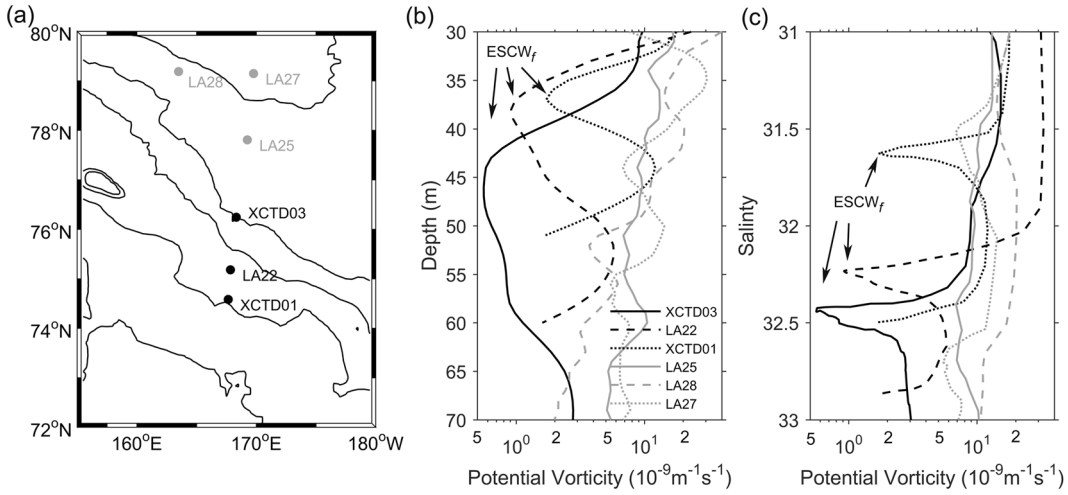

Figure 6. (a) Station locations along the continental shelf and slope. (b) PV profiles on the shelf and slope of the East Siberian Sea. (c) PV-salinity plots of the stations in (a).

4.2. Production of ESCW$_f$

During summer in the ESS, freshwater input by sea ice melt and river runoff causes significant salinity decrease in the MLW. However, observations show that even in September the salinity of MLW around the mid shelf can still maintain around 30.0–30.5 (Figures 3c and 3d). Comparing with the mean salinity ~32.0 of ESCW$_f$, a salinity increase of 2.0 is sufficient for the MLW to be transformed into ESCW$_f$ during the subsequent winter. This relationship provides us an opportunity to identify the possible source of ESCW$_f$ in the ESS.

During winter, lateral water exchange on the continental shelf weakens significantly because river runoff is negligible. Thus, we assume that all the increase in the water column's salinity is caused by brine injection as sea ice freezes. Taking the surface mixed layer thickness as 27.5 m and the salinity of new sea ice as 6.0 based on the observations in 2016, we can infer that the needed sea ice growth to produce the ESCW$_f$ is about 1.75 m. The mean thickness of the first-year sea ice in the ESS has been about 1.5 m (Kwok, 2018), and the total production of sea ice should be larger if taking into account the ridging and rafting processes. This means that the condition to produce ESCW$_f$ can be achieved simply by the annual growth of sea ice on the mid-shelf, which offers an explanation for the wide distribution of ESCW$_f$ there. As a comparison, the ESCW$_s$ with higher salinity was mainly found on the outer shelf close to the New Siberian Islands where coastal polynyas could provide sufficient supply of brine injection during wintertime.

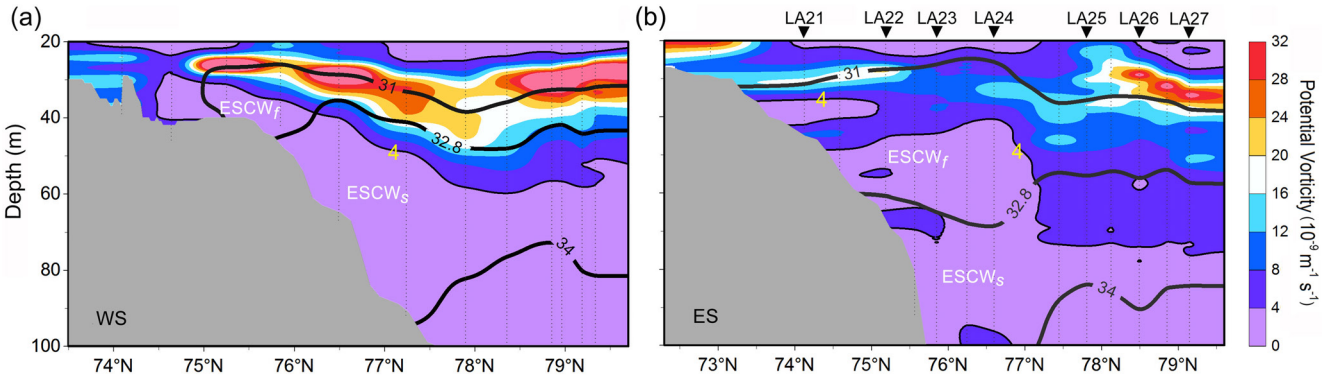

Figure 7. PV along sections (a) western section and (b) eastern section. PV contour of 4.0×10^{-9} m^{-1}s^{-1} (thin line with yellow numbers), and salinity contours of 31.0, 32.8 and 34.0 (thick line) are shown.

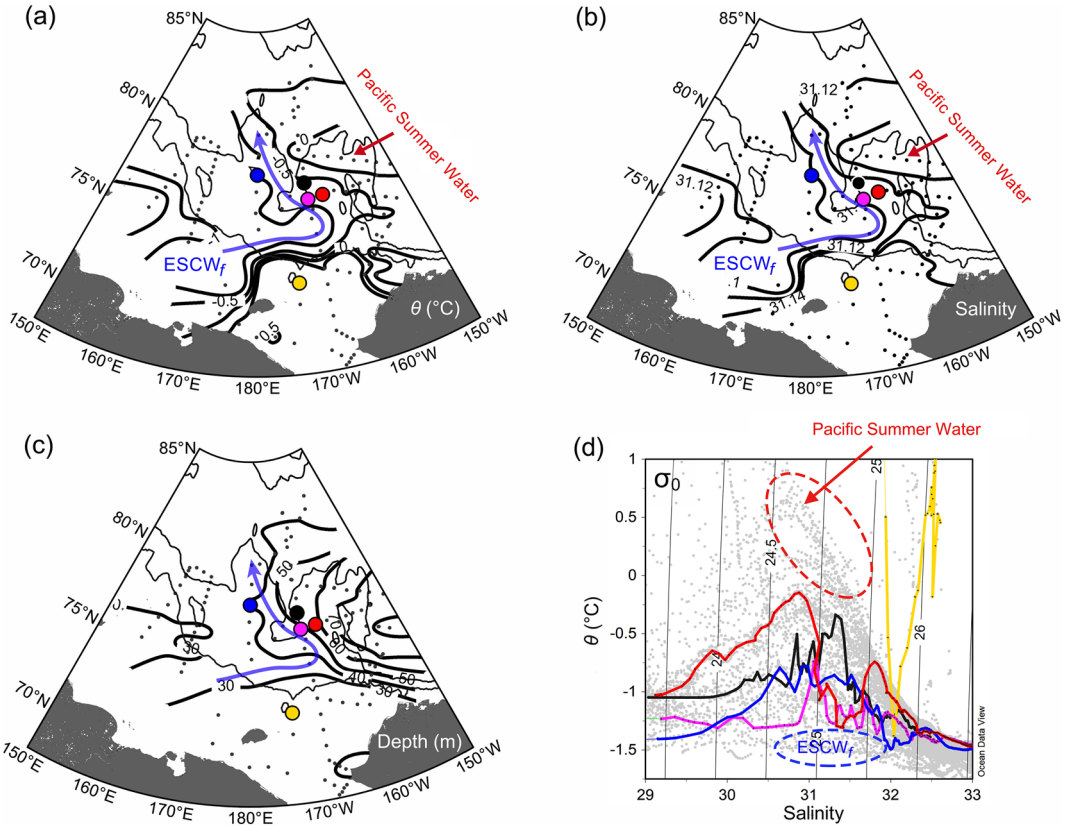

Figure 8. (a) Potential temperature, (b) salinity, and (c) depth on the isopycnal of $\sigma_0 = 25.0$ kg/m^3. The thin black lines denote the 100- and 2,000-m isobaths, respectively. (c) Station locations for data used in (d). (d) θ-S diagram of Conductivity, Temperature, Depth observations from (c).

4.3. Transport of ESCW$_f$ Into the Amerasian Basin

To reveal the transport of shelf waters in the ESS, we chose ESCW$_f$($\theta < -1$°C, $31 < S < 32.8$) as a representative water mass sub-type to track. The ESCW$_f$ is isolated from the surface forcing by the seasonal pycnocline so that it can be easily traced by its temperature-salinity relationship. The density of ESCW$_f$ is similar to the Pacific Summer Water, and they both occupied a subsurface layer of 40–100-m depth. However, the temperature of ESCW$_f$ is near-freezing, which is distinct from the Pacific Summer Water with a temperature maximum (−0.5–0.5°C) in the Canada Basin (Steele et al., 2004; Timmermans et al., 2014).

The density of ESCW$_f$ mainly lay in the potential density range of 24.0–26.0 kg/m^3 (Figure 2d). We use the median value of 25.0 kg/m^3 as an example. From the temperature and salinity distributions along the reference isopycnal (Figures 8a and 8b), we find that ESCW$_f$ was transported from the central ESS toward the Chukchi Plateau and penetrated into the subsurface layer of the Chukchi Abyssal Plain. This pattern confirmed the speculation of Nishino et al. (2013) and Alkire et al. (2019) that the ESS is a source of the near-freezing halocline water in the Makarov Basin.

After entering the basin, the ESCW$_f$ occupied the layer of 40–70-m depth (Figure 8c). It encountered the Pacific Summer Water ($\theta > -0.5$°C, $S > 31.12$), which was distributed in the northern Chukchi Plateau, forming a subsurface oceanic front stretching along the Chukchi Plateau, Chukchi Abyssal Plain and northern side of the Mendeleev Ridge. Apparent interleaving between the ESCW$_f$ and Pacific Summer Water was observed (Figure 8d), which was previously used as a tracer to infer converging water masses by Rudels et al. (2000), denoting the position of the subsurface front.

In the summer of 2016, the center of the Beaufort High moved from its usual location in the southern Canada Basin to the Chukchi Sea. At the same time, the SLP in the central Arctic was relatively low, promoting a cyclonic atmospheric circulation in the Eurasian Basin (Figure 9a). As a result, the overall southwesterly

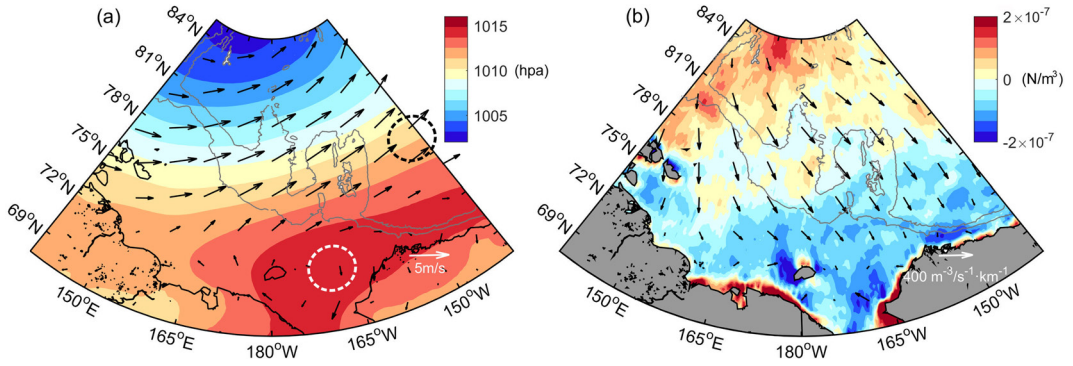

Figure 9. (a) Mean sea-level pressure and (b) mean wind stress curl in the Pacific sector of the Arctic Ocean from 1 July to September 15, 2016. The center of Beaufort High is marked by the dashed white circle, and its climatological mean position is marked by the dashed black circle. The gray lines denote the 200- and 2,000-m isobaths, respectively. Arrows in (a) represent the mean 10-m wind field, and those in (b) represent the Ekman transport. The daily meteorological parameters used here are from the ERA-5 reanalysis data. The calculation of Ekman transport refers to Gomez-Gesteira et al. (2006).

wind field induced a negative wind stress curl on the shelves of the Pacific sector (69°–76°N, Figure 9b), and a surface Ekman transport toward the Chukchi Plateau. This transport promoted the accumulation of river runoff along the inner shelf and, eventually, intensified the buoyancy-forced eastward transport in the ESS. When arriving at the Long Strait, the shelf waters from the ESS encountered the Pacific inflow, and then turned northward along with the western boundary of the Pacific inflow.

5. Impacts on the Arctic Halocline

5.1. A Source for the Cold Halocline Waters in the Makarov Basin

On the outer shelf of section ES, the seasonal thermocline had a staircase-like structure, with each layer being about 10–15 m thick (Figure 10). The θ-S diagram shows that the water properties in each layer were almost same as those of the ESCW to the south, indicating that the observed staircase-like structure was formed by an intrusion of ESCW during the time when it was transported northward.

This phenomenon provides an insight to how the ESCW contributes to the Arctic halocline in the Makarov Basin. In summer, the staircase-like structure resulting from advection cannot be maintained on the shallow inner shelf due to wind-induced mixing. However, when an intrusion occurs in the subsurface of the outer shelf and continental slope where vertical mixing was significantly reduced by the cover of melt water, the staircase-like structure can be transformed gradually to form an original cold halocline with salinities of about 30.0–33.0. In this way, the advection of ESCW eventually feeds the THW and UHW in the Makarov Basin, as shown in Figure 11. This process of halocline formation is different from those in the Pacific sector of the Arctic Ocean, for example, the regional freshening by ice melt (Kikuchi et al., 2004), or the intrusion of Pacific-origin waters in the Canada Basin (Steele & Boyd, 1998).

5.2. Production of D-LHW in the ESS

The D-LHW was observed at stations LA23, LA24 and XCTD03 in section ES, characterized by the presence of θ-S points along the diapycnal mixing line between $ESCW_s$ and AW (Figure 12a, along the mixing line between 33.5 and 34.5), indicating that its formation was related to the mixture of the two water masses. As the result, the D-LHW (−1.1–0.5°C) was about 0.5°C warmer than the LHW nearby due to the increased component of AW.

In section ES, D-LHW was distributed on top of AW from the outer shelf to the slope, occupying a near-bottom layer between 90 and 150-m depth (Figures 13a, 13c and 13e). However, D-LHW was absent in the section WS (Figures 13b, 13d and 13f). Why did the D-LHW occur only in section ES? Lin et al. (2019) pointed out that a positive wind stress curl would cause surface divergence in the Beaufort Sea, which would

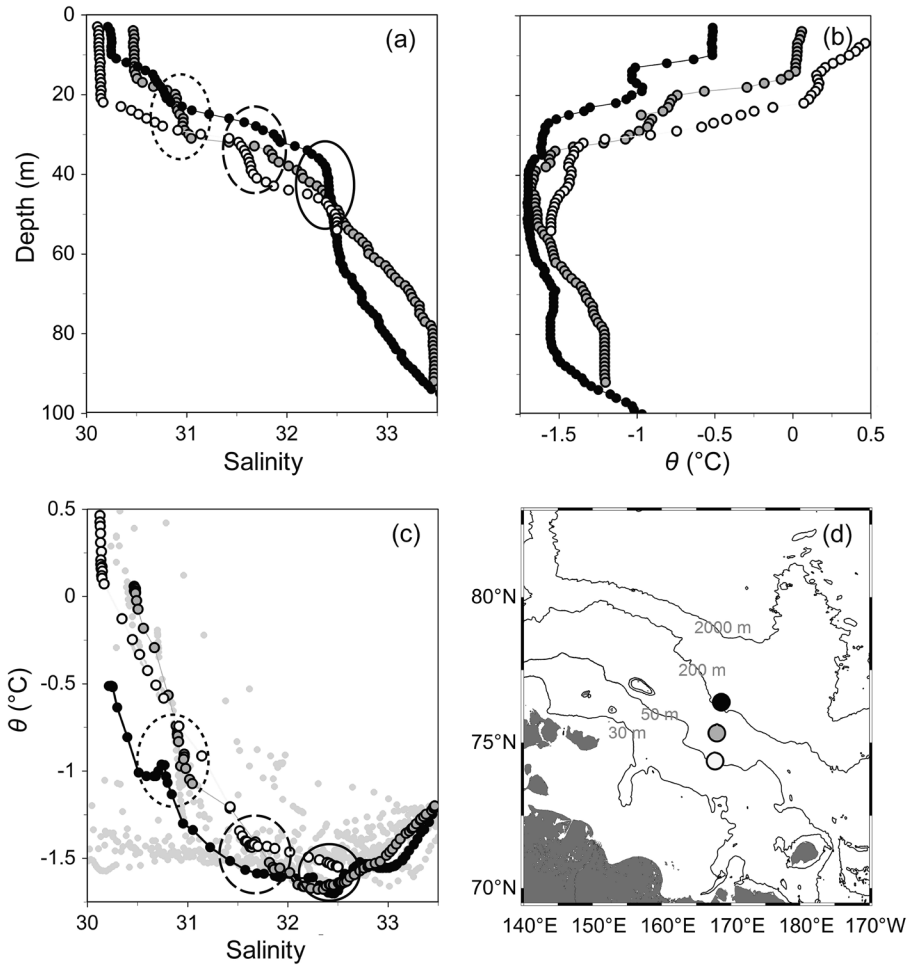

Figure 10. (a) Salinity and (b) potential temperature profiles at the stations on the outer shelf of the East Siberian Sea (ESS). (c) θ-S diagram of the Conductivity, Temperature, Depth profiles in the ESS. (d) Locations of the three profiles in (a–c). Water masses in each sublayer of the staircase-like structure with similar properties are circled by solid, dashed, and short-dashed lines, respectively.

promote the formation of D-LHW by inducing AW to upwell and mix with the Pacific-origin water above. During the survey in 2016, the wind stress curl was positive along the shelves of WS and ES (Figure 14a). However, the D-LHW was only formed in section ES where the wind stress curl was also negative to the north of the shelf. The upper boundary of AW (taking −0.5°C as the reference) on the slope is as shallow as

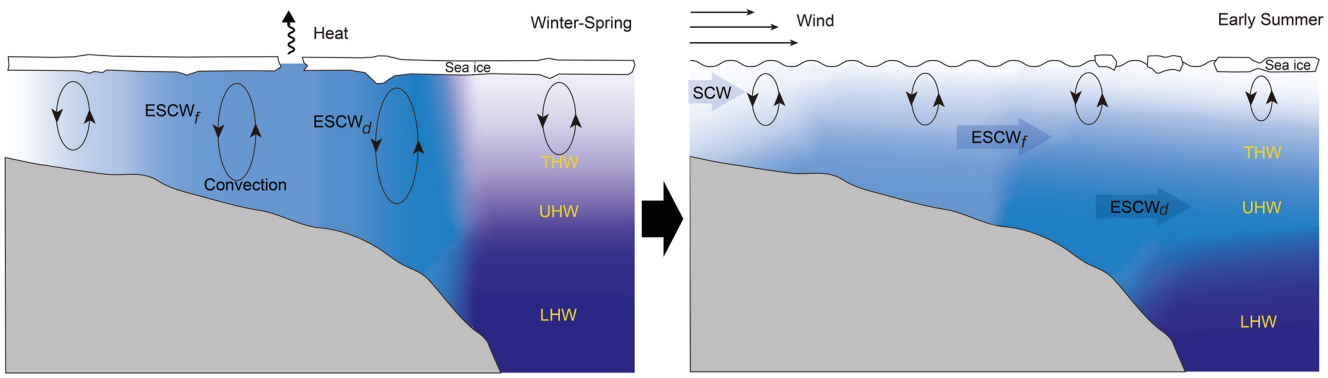

Figure 11. A sketch showing how the offshore advection and overlying of cold shelf waters contribute to upper halocline formation.

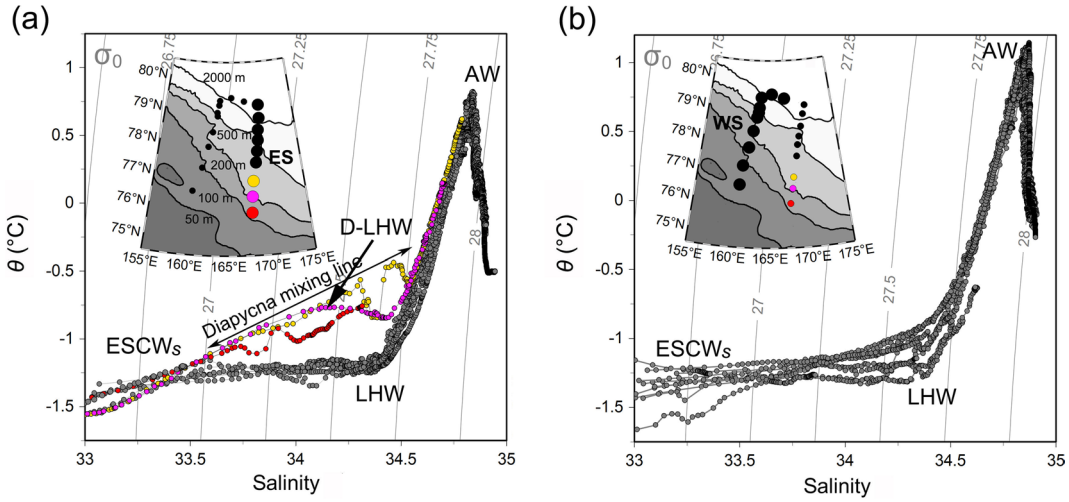

Figure 12. Scatter plots of the Conductivity, Temperature, Depth (CTD) data in the (a) eastern section and (b) western section. Black contours denote 50-, 100-, 200-, 500-, and 2,000-m isobaths; red, pink, and yellow dots denote stations LA23, XCTD03, and LA24, respectively.

150 m (Figure 13a), which is the general depth of AW in the Beaufort Sea under a positive wind stress curl (Lin et al., 2019). Therefore, we argue that because of the shallow distribution of AW in the Makarov Basin, the wind stress curl is not a major factor in D-LHW formation.

As well as AW, production of D-LHW also requires a cold and relatively fresh water mass with which the AW can mix. Along the slope of the Beaufort and Chukchi seas, Pacific Winter Water with salinities of 33.0–33.3 can provide such a source (Lin et al., 2019; Pickart et al., 2005). However, in the ESS, LHW occupied the bottom of the outer shelf in section WS (Figure 5a), which isolated ESCW$_s$ from being mixed with lower AW. As a comparison, the D-LHW was formed along the bottom of section ES where the LHW had disappeared from the shelf (Figure 5b).

Before the surveys, wind in the ESS had been persistently southerly for about two weeks, leading to a rapid ice retreat from the east side of the ESS shelf (Figure 14b). At the same time, a cyclonic circulation on the shelf was forced by a combination of buoyancy forcing and Ekman transport, leading to the transport of shelf waters from the shelf into the basin as presented in Section 4.3. This dynamical pattern suggests that the offshore transport of ESCW was a major reason for the D-LHW formation on the outer shelf and slope of the ESS in 2016. During this process, there are two conditions favoring offshore transport. First, the offshore transport of ESCW caused an intrusion of AW along the slope bottom to break down the isolation of LHW. Second, the transport provided sufficient cold and fresh waters (i.e., the ESCW) for intruded AW to be mixed with on the outer shelf. Eventually, strong diapycnal mixing of the AW and ESCW, which was also enhanced by the tides around the shelf break (Rippeth et al., 2015), formed the D-LHW on the bottom. The upward mixing of AW also caused a rapid heat loss with the maximum value exceeding 60 W/m^2, increasing heat content on the bottom of the outer shelf.

6. Summary and Discussion

This study presents the property and distribution of East Siberian cold shelf water (ESCW) during two hydrographic cruises in the Pacific sector of the Arctic in summer 2016. Beneath the surface mixed layer, the ESCW had a wide salinity range from 30.0 to 34.0 with temperature below −1°C. We found that the relatively fresh form of ESCW, that is, ESCW$_f$ ($31.0 < S < 32.8$), occupied a layer in the depth range 30–70 m with a meridional width of nearly 400 km on the shelf. The necessary condition for ESCW$_f$ to be produced was sea ice growth of 1.75 m, which is consistent with annual production of first-year sea ice in the ESS. This explains the wide distribution of ESCW$_f$ on the mid-shelf. In contrast, the saltier ESCW$_s$ ($32.8 < S < 34.0$), whose production requires additional brine injection from coastal polynyas, was mainly distributed in the western ESS close to the New Siberian Islands (Anderson et al., 2017).

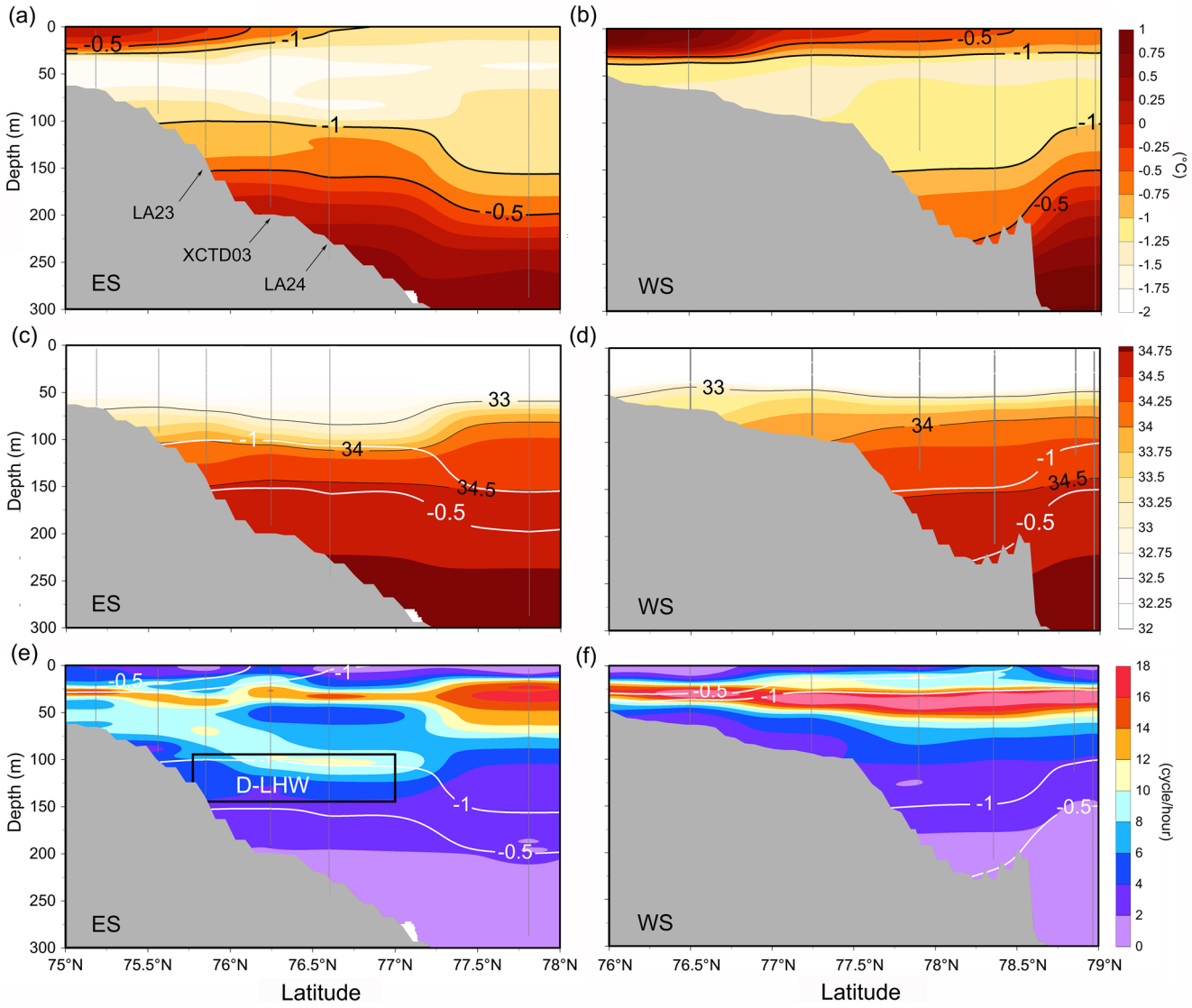

Figure 13. (a) and (b) show the potential temperature along the outer shelf and continental slope of eastern section (ES) and western section (WS), respectively. (c) and (d) show the salinity along sections ES and WS, respectively. (e) and (f) show the Brunt-Vaisala frequency along sections ES and WS, respectively. Temperature contours of −0.5 and −1.0°C (white line) are shown; the location of D-LHW is marked by black rectangle.

The ESCW$_f$ was transported northeastward to the Chukchi Plateau in the summer of 2016. After entering the Chukchi Abyssal Plain, it occupied the subsurface layer of depths of 30–60 m. The easternmost part of ESCW$_f$ penetrated the Chukchi Plateau until it encountered the Pacific Summer Water to form a subsurface oceanic front, which stretched along the Chukchi Plateau and northern side of the Mendeleev Ridge.

Related to the offshore transport of ESCW, we found that the diapycnally mixed Lower Halocline Water (D-LHW) was formed by a mixture of ESCW and Atlantic Water (AW) at the bottom of the outer shelf in the ESS. The source of D-LHW in the Arctic Pacific sector can be extended from the Chukchi Plateau to as far as the Makarov Basin.

Rudels et al. (2004) pointed out that the lower half of the halocline (with salinities of 33.5–34.5) in the Nansen Basin was distinct from that in the Canada Basin. The former showed a cold state with temperature near freezing (i.e., the LHW), whereas the latter showed a warm state with temperature increasing with depth. It is well known that the upward mixing of AW leads to the modification of the lower halocline (Alkire et al., 2017; Bauch et al., 2016; Dmitrenko et al., 2011); however, where the modification takes place remains unclear. Our observations show that the eastern slope of the ESS (~169°E) was the westernmost

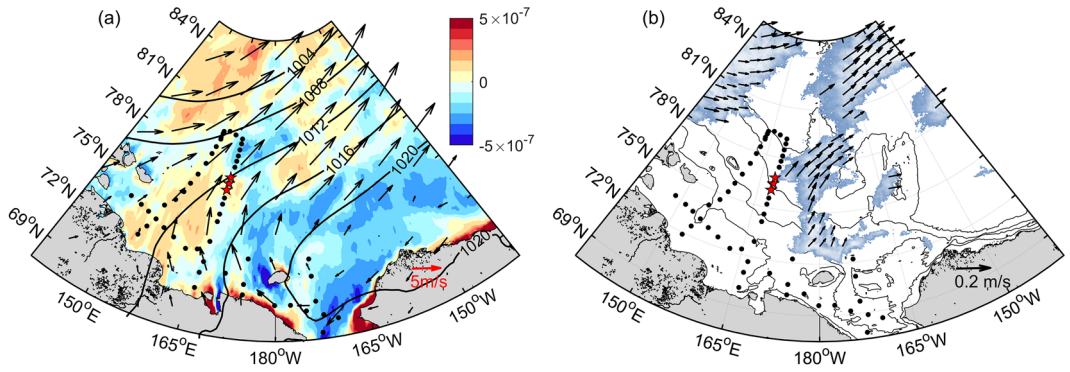

Figure 14. (a) Mean wind stress curl from 19 August to September 3, 2016. Black arrows are the 10-m wind field; Black contours denote the sea-level pressure (hpa); red stars denote the locations where the D-LHW was observed. (b) Sea ice motion during the same period. Steel blue shadow denotes the sea ice extent; black contours denote 30-, 50-, 200-, and 2,000-m isobaths, respectively.

site where the warm lower halocline (i.e., the D-LHW) was found and no cold lower halocline (i.e., the LHW) was found to exist to the east of the Mendeleev Ridge. This suggests that the transition zone between the "cold" and "warm" lower haloclines was probably located in the ESS, and the ESS and Mendeleev Ridge were important regions for halocline transformation. Note that in some years the LHW could be transported into the Chukchi Abyssal Plain by crossing the Mendeleev Ridge (Woodgate et al., 2005), leading to the major transformation region being in the western Chukchi Plateau. More observations are required to better understand the mechanisms controlling the distributions of the two haloclines.

In the subsurface of the Makarov Basin, a near-freezing temperature water type (S: 31.5–32.8, θ: ~−1.5°C) has been observed since 2008 (Nishino et al., 2013). Based on the chemical evidence that the NO (a semi-conservative chemical parameter defined as $NO = (9 \times NO_3^-) + O_2$) of the water is lower than that of the Pacific-origin water in the Canada Basin, Nishino et al. (2008) and Alkire et al. (2019) suggested that the near-freezing temperature water was formed in the ESS. Our surveys in the ESS and Makarov Basin in 2016 provide evidence to support this speculation that the ESS was a major source of the near-freezing temperature water for the Makarov Basin. In addition, we found that the advection of ESCW during wintertime would contribute to feeding the cold halocline (30.0–33.0) in the subsurface of the Makarov Basin.

In summer 2016 during our cruises reported here, Arctic cyclone activity was high and sea level pressure in the central Arctic was relatively low (Yamagami et al., 2017), which enhanced the cyclonic component of the atmospheric circulation. Under such a situation, we observed an overall west-to-east transport of shelf waters across the ESS and subsequently into the Amerasian Basin, indicating an eastward movement of the Transpolar Drift toward the Mendeleev Ridge (Figure 15). Our 1-year observations show that the zonal volume flux of the surface low-salinity water (<30 m) in the ESS was about 0.6 Sv under this cyclonic atmospheric condition. There exist two opposite speculated patterns of water transport across the ESS: the west-to-east transport under a cyclonic atmospheric condition and the east-to-west transport under an anticyclonic condition (I. Dmitrenko et al., 2005; I. A. Dmitrenko et al., 2008; Proshutinsky et al., 2015). Here, we reveal a preliminary flux estimate for the cyclonic condition based on one-year observations, which highlights the role of the ESS in the freshwater budgets of both the Amerasian and Eurasian basins. More observations are required to further evaluate the different influences of water transport on freshwater budget between the two atmospheric conditions.

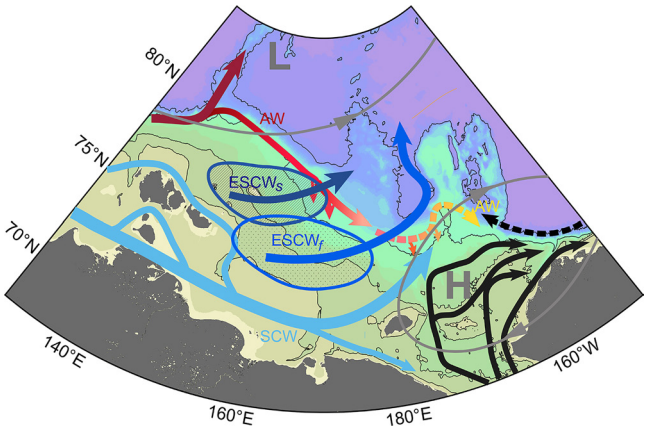

Figure 15. Schematic diagram of water transport in the East Siberian Sea. Gray lines denote the atmospheric circulation under a weakened Beaufort High (H) and a dominant Arctic Low (L). Black contours denote 30-, 50-, 200-, and 2,000-m isobaths, respectively; black arrows denote the pathway of summer Bering waters from Corlett and Pickart (2017).

Although the freshwater content in the Beaufort Gyre showed an apparent increase from 2015 to 2016 (Proshutinsky et al., 2019), we cannot conclude that the transport of shelf waters from the ESS was related to

this change in the freshwater content. The balance of fresh water in the Amerasian Basin is also strongly controlled by the anticyclonic Beaufort Gyre (Charette et al., 2020; Zhong et al., 2019), which is beyond the scope of this study. Lateral exchange between the Transpolar Drift and Beaufort Gyre probably accounts for part of the freshwater balance along the Mendeleev Ridge.

Data Availability Statement

The CTD data analyzed in this study can be obtained at the following website: https://doi.org/10.5281/zenodo.4507584. ERA5 data are available at the Copernicus Climate Change Service (C3S) Climate Data Store: https://cds.climate.copernicus.eu/cdsapp#!/dataset/reanalysis-era5-single-levels?tab=form. Absolute dynamic topography data are available at the following website: https://resources.marine.copernicus.eu/?option=com_csw&view=details&product_id=SEALEVEL_GLO_PHY_L4_REP_OBSERVATIONS_008_047. Sea ice data is from the Ice Data Center of Bremen University (https://seaice.uni-bremen.de/data/amsr2/asi_daygrid_swath/n6250/2016/). Some figures are illustrated using Ocean Data View software (Schlitzer, Reiner, Ocean Data View, https://odv.awi.de, 2020).

Acknowledgments
We would like to thank the crew of Russian *R/V Akademik M. A. Lavrentyev* and of Chinese *R/V Xuelong* for their excellent work. We also thank two anonymous reviewers whose comments improved this paper. This study is funded by the National Key R&D Program of China (Grant 2019YFA0607001), the Chinese Natural Science Foundation (Grant 41941012) and POI FEB RAS research theme (No. 0271-2019-0003). Support from the China-Russia Joint Research Center for Ocean and Climate is highly appreciated.

References

Aagaard, K., Coachman, L. K., & Carmack, E. (1981). On the halocline of the Arctic Ocean. *Deep Sea Research Part A. Oceanographic Research Papers*, *28*(6), 529–545. https://doi.org/10.1016/0198-0149(81)90115-1

Aksenov, Y., Ivanov, V., Nurser, G., Bacon, S., Polyakov, I., Coward, A., et al. (2011). The Arctic circumpolar boundary current. *Journal of Geophysical Research*, *116*. https://doi.org/10.1029/2010JC006637

Alkire, M. B., Polyakov, I., Rember, R., Pnyushkov, A., Ivanov, V., & Ashik, I. (2017). Combining physical and geochemical methods to investigate lower halocline water formation and modification along the Siberian continental slope. *Ocean Science*, *13*(6), 983–995. https://doi.org/10.5194/os-13-983-2017

Alkire, M. B., Rember, R., & Polyakov, I. (2019). Discrepancy in the Identification of the Atlantic/Pacific Front in the Central Arctic Ocean: NO versus nutrient relationships. *Geophysical Research Letters*, *46*(7), 3843–3852. https://doi.org/10.1029/2018GL081837

Anderson, L. G., Andersson, P. S., Björk, G., Peter Jones, E., Jutterström, S., & Wåhlström, I. (2013). Source and formation of the upper halocline of the Arctic Ocean. *Journal of Geophysical Research: Oceans*, *118*(1), 410–421. https://doi.org/10.1029/2012JC008291

Anderson, L. G., Björk, G., Holby, O., Jutterström, S., Magnus Mörth, C., O'Regan, M., et al. (2017). Shelf-Basin interaction along the East Siberian Sea. *Ocean Science*, *13*(2), 349–363. https://doi.org/10.5194/os-13-349-2017

Bauch, D., Cherniavskaia, E., & Timokhov, L. (2016). Shelf basin exchange along the Siberian continental margin: Modification of Atlantic Water and Lower Halocline Water. *Deep Sea Research Part I: Oceanographic Research Papers*, *115*, 188–198. https://doi.org/10.1016/j.dsr.2016.06.008

Bauch, D., Erlenkeuser, H., & Andersen, N. (2005). Water mass processes on Arctic shelves as revealed from $\delta^{18}O$ of H_2O. *Global and Planetary Change*, *48*(1), 165–174. https://doi.org/10.1016/j.gloplacha.2004.12.011

Bauch, D., Gröger, M., Dmitrenko, I., Hölemann, J., Kirillov, S., Mackensen, A., et al. (2011). Atmospheric controlled freshwater release at the Laptev Sea continental margin. *Polar Research*, *30*(1), 5858. https://doi.org/10.3402/polar.v30i0.5858

Bauch, D., Hölemann, J. A., Dmitrenko, I. A., Janout, M. A., Nikulina, A., Kirillov, S. A., et al. (2012). Impact of Siberian coastal polynyas on shelf-derived Arctic Ocean halocline waters. *Journal of Geophysical Research*, *117*(C9). https://doi.org/10.1029/2011JC007282

Bauch, D., Torresvaldes, S., Polyakov, I., Novikhin, A., Dmitrenko, I., Mckay, J., & Mix, A. (2014). Halocline water modification and along slope advection at the Laptev Sea continental margin. *Ocean Science*, *10*(1), 141–154. https://doi.org/10.5194/os-10-141-2014

Baumann, T. M., Polyakov, I. V., Pnyushkov, A. V., Rember, R., Ivanov, V. V., Alkire, M. B., et al. (2018). On the seasonal cycles observed at the continental slope of the Eastern Eurasian Basin of the Arctic Ocean. *Journal of Physical Oceanography*, *48*(7), 1451–1470. https://doi.org/10.1175/JPO-D-17-0163.1

Björk, G., Söderkvist, J., Winsor, P., Nikolopoulos, A., & Steele, M. (2002). Return of the cold halocline layer to the Amundsen Basin of the Arctic Ocean: Implications for the sea ice mass balance. *Geophysical Research Letters*, *29*, 1–8. https://doi.org/10.1029/2001GL014157

Boyd, T., Steele, M., Muench, R., & Gunn, J. (2002). Partial recovery of the Arctic Ocean halocline. *Geophysical Research Letters*, *29*, 1657. https://doi.org/10.1029/2001GL014047

Carmack, E. C., Yamamoto-Kawai, M., Haine, T. W. N., Bacon, S., Bluhm, B. A., Lique, C., et al. (2016). Freshwater and its role in the Arctic Marine System: Sources, disposition, storage, export, and physical and biogeochemical consequences in the Arctic and global oceans. *Journal of Geophysical Research: Biogeosciences*, *121*(3), 675–717. https://doi.org/10.1002/2015JG003140

Chapman, D. C., & Lentz, S. J. (1994). Trapping of a coastal density front by the bottom boundary layer. *Journal of Physical Oceanography*, *24*(7), 1464–1479. https://doi.org/10.1175/1520-0485(1994)024<1464:TOACDF>2.0.CO;2

Charette, M. A., Kipp, L. E., Jensen, L. T., Dabrowski, J. S., Whitmore, L. M., Fitzsimmons, J. N., et al. (2020). The transpolar drift as a source of riverine and shelf-derived trace elements to the central Arctic Ocean. *Journal of Geophysical Research: Oceans*, *125*(5), e2019J. https://doi.org/10.1029/2019JC015920

Corlett, W. B., & Pickart, R. S. (2017). The Chukchi slope current. *Progress in Oceanography*, *153*, 50–65. https://doi.org/10.1016/j.pocean.2017.04.005

Dmitrenko, I., Kirillov, S., Eicken, H., & Markova, N. (2005). Wind-driven summer surface hydrography of the eastern Siberian shelf. *Geophysical Research Letters*, *32*(14). https://doi.org/10.1029/2005GL023022

Dmitrenko, I. A., Ivanov, V. V., Kirillov, S. A., Vinogradova, E. L., Torres-Valdes, S., & Bauch, D. (2011). Properties of the Atlantic derived halocline waters over the Laptev Sea continental margin: Evidence from 2002 to 2009. *Journal of Geophysical Research*, *116*(C10). https://doi.org/10.1029/2011JC007269

Dmitrenko, I. A., Kirillov, S. A., & Tremblay, L. B. (2008). The long-term and interannual variability of summer fresh water storage over the eastern Siberian shelf: Implication for climatic change. *Journal of Geophysical Research*, *113*(C3). https://doi.org/10.1029/2007JC004304

Gomez-Gesteira, M., Moreira, C., Alvarez, I., & DeCastro, M. (2006). Ekman transport along the Galician coast (northwest Spain) calculated from forecasted winds. *Journal of Geophysical Research*, *111*(C10). https://doi.org/10.1029/2005JC003331

Gong, D., & Pickart, R. S. (2016). Early summer water mass transformation in the eastern Chukchi Sea. *Deep Sea Research Part II: Topical Studies in Oceanography*, *130*, 43–55. https://doi.org/10.1016/j.dsr2.2016.04.015

Hersbach, H., Bell, B., Berrisford, P., Biavati, G., Horányi, A., Muñoz Sabater, J., et al. (2018). *ERA5 hourly data on single levels from 1979 to present*. Copernicus Climate Change Service (C3S) Climate Data Store (CDS). https://doi.org/10.24381/cds.adbb2d47

Itoh, M., Carmack, E., Shimada, K., McLaughlin, F., Nishino, S., & Zimmermann, S. (2007). Formation and spreading of Eurasian source oxygen-rich halocline water into the Canadian Basin in the Arctic Ocean. *Geophysical Research Letters*, *340*. https://doi.org/10.1029/2007GL029482

Jackson, J. M., Carmack, E. C., McLaughlin, F. A., Allen, S. E., & Ingram, R. G. (2010). Identification, characterization, and change of the near-surface temperature maximum in the Canada Basin, 1993–2008. *Journal of Geophysical Research*, *115*(C5). https://doi.org/10.1029/2009JC005265

Johnson, M. A., & Polyakov, I. V. (2001). The Laptev Sea as a source for recent Arctic Ocean salinity changes. *Geophysical Research Letters*, *28*(10), 2017–2020. https://doi.org/10.1029/2000GL012740

Jones, E. P., & Anderson, L. G. (1986). On the origin of the chemical properties of the Arctic Ocean halocline. *Journal of Geophysical Research*, *91*(C9), 10759–10767. https://doi.org/10.1029/JC091iC09p10759

Jones, E. P., Anderson, L. G., Jutterström, S., Mintrop, L., & Swift, J. H. (2008). Pacific freshwater, river water and sea ice meltwater across Arctic Ocean basins: Results from the 2005 Beringia Expedition. *Journal of Geophysical Research*, *113*(C8), C8012. https://doi.org/10.1029/2007JC004124

Katsura, S. (2018). Properties, formation, and dissipation of the North Pacific Eastern Subtropical Mode Water and its impact on interannual spiciness anomalies. *Progress in Oceanography*, *162*, 120–131. https://doi.org/10.1016/j.pocean.2018.02.023

Kawaguchi, Y., Steele, M., Colburn, K., Nishino, S., & Oshima, K. (2015). Upper Ocean Heat Observation using UpTempO buoys during RV Mirai Arctic cruise MR14-05. *JAMSTEC Report of Research and Development*, *21*, 1–6. https://doi.org/10.5918/jamstecr.21.1

Kikuchi, T., Hatakeyama, K., & Morison, J. H. (2004). Distribution of convective Lower Halocline Water in the eastern Arctic Ocean. *Journal of Geophysical Research*, *109*(C12). https://doi.org/10.1029/2003JC002223

Kwok, R. (2018). Arctic sea ice thickness, volume, and multiyear ice coverage: Losses and coupled variability (1958–2018). *Environmental Research Letters*, *13*(10), 105005. https://doi.org/10.1088/1748-9326/aae3ec

Lin, P., Pickart, R. S., Moore, G. W. K., Spall, M. A., & Hu, J. (2019). Characteristics and dynamics of wind-driven upwelling in the Alaskan Beaufort Sea based on six years of mooring data. *Deep Sea Research Part II: Topical Studies in Oceanography*, *162*, 79–92. https://doi.org/10.1016/j.dsr2.2018.01.002

Linders, J., Pickart, R. S., Björk, G., & Moore, G. W. K. (2017). On the nature and origin of water masses in Herald Canyon, Chukchi Sea: Synoptic surveys in summer 2004, 2008, and 2009. *Progress in Oceanography*, *159*, 99–114. https://doi.org/10.1016/j.pocean.2017.09.005

McLaughlin, F. A., Carmack, E. C., Macdonald, R. W., & Bishop, J. K. B. (1996). Physical and geochemical properties across the Atlantic/Pacific water mass front in the southern Canadian Basin. *Journal of Geophysical Research*, *101*(C1), 1183–1197. https://doi.org/10.1029/95JC02634

McLaughlin, F. A., Carmack, E. C., Macdonald, R. W., Melling, H., Swift, J. H., Wheeler, P. A., et al. (2004). The joint roles of Pacific and Atlantic-origin waters in the Canada Basin, 1997–1998. *Deep Sea Research Part I: Oceanographic Research Papers*, *51*(1), 107–128. https://doi.org/10.1016/j.dsr.2003.09.010

Meneghello, G., Marshall, J., Timmermans, M., & Scott, J. (2018). Observations of seasonal upwelling and downwelling in the Beaufort Sea mediated by Sea Ice. *Journal of Physical Oceanography*, *48*(4), 795–805. https://doi.org/10.1175/JPO-D-17-0188.1

Morison, J., Kwok, R., Peralta-Ferriz, C., Alkire, M., Rigor, I., Andersen, R., & Steele, M. (2012). Changing Arctic Ocean freshwater pathways. *Nature*, *481*(7379), 66–70. https://doi.org/10.1038/nature10705

Morison, J., Steele, M., & Andersen, R. (1998). Hydrography of the upper Arctic Ocean measured from the nuclear submarine U.S.S. Pargo. *Deep Sea Research Part I: Oceanographic Research Papers*, *45*(1), 15–38. https://doi.org/10.1016/S0967-0637(97)00025-3

Münchow, A., Weingartner, T. J., & Cooper, L. W. (1999). The summer hydrography and surface circulation of the East Siberian Shelf Sea. *Journal of Physical Oceanography*, *29*(9), 2167–2182. https://doi.org/10.1175/1520-0485(1999)029<2167:TSHASC>2.0.CO;2

Nikolopoulos, A., Pickart, R. S., Fratantoni, P. S., Shimada, K., Torres, D. J., & Jones, E. P. (2009). The western Arctic boundary current at 152°W: Structure, variability, and transport. *Deep Sea Research Part II: Topical Studies in Oceanography*, *56*(17), 1164–1181. https://doi.org/10.1016/j.dsr2.2008.10.014

Nishino, S., Itoh, M., Williams, W. J., & Semiletov, I. (2013). Shoaling of the nutricline with an increase in near-freezing temperature water in the Makarov Basin. *Journal of Geophysical Research: Oceans*, *118*(2), 635–649. https://doi.org/10.1029/2012JC008234

Nishino, S., Shimada, K., Itoh, M., Yamamoto-Kawai, M., & Chiba, S. (2008). East–west differences in water mass, nutrient, and chlorophyll a distributions in the sea ice reduction region of the western Arctic Ocean. *Journal of Geophysical Research: Oceans*, *113*(C1). https://doi.org/10.1029/2007JC004666

Okkonen, S., Ashjian, C., Campbell, R. G., & Alatalo, P. (2019). The encoding of wind forcing into the Pacific-Arctic pressure head, Chukchi Sea ice retreat and late-summer Barrow Canyon water masses. *Deep Sea Research Part II: Topical Studies in Oceanography*, *162*, 22–31. https://doi.org/10.1016/j.dsr2.2018.05.009

Osadchiev, A. A., Pisareva, M. N., Spivak, E. A., Shchuka, S. A., & Semiletov, I. P. (2020). Freshwater transport between the Kara, Laptev, and East-Siberian seas. *Scientific Reports*, *10*(1), 13041. https://doi.org/10.1038/s41598-020-70096-w

Pickart, R. S., Spall, M. A., Moore, G. W. K., Weingartner, T. J., Woodgate, R. A., Aagaard, K., & Shimada, K. (2011). Upwelling in the Alaskan Beaufort Sea: Atmospheric forcing and local versus non-local response. *Progress in Oceanography*, *88*(1), 78–100. https://doi.org/10.1016/j.pocean.2010.11.005

Pickart, R. S., Weingartner, T. J., Pratt, L. J., Zimmermann, S., & Torres, D. J. (2005). Flow of winter-transformed Pacific water into the Western Arctic. *Deep Sea Research Part II: Topical Studies in Oceanography*, *52*(24), 3175–3198. https://doi.org/10.1016/j.dsr2.2005.10.009

Polyakov, I. V., Pnyushkov, A. V., & Carmack, E. C. (2018). Stability of the arctic halocline: A new indicator of arctic climate change. *Environmental Research Letters*, *13*(12), 125008. https://doi.org/10.1088/1748-9326/aaec1e

Proshutinsky, A., Dukhovskoy, D., Timmermans, M., Krishfield, R., & Bamber, J. L. (2015). Arctic circulation regimes. *Philosophical Transactions of the Royal Society A: Mathematical, Physical & Engineering Sciences*, *373*(2052), 20140160. https://doi.org/10.1098/rsta.2014.0160

Proshutinsky, A., Krishfield, R., Toole, J. M., Timmermans, M. L., Williams, W., Zimmermann, S., et al. (2019). Analysis of the Beaufort Gyre freshwater content in 2003–2018. *Journal of Geophysical Research: Oceans*, *124*(12), 9658–9689. https://doi.org/10.1029/2019JC015281

Rippeth, T. P., Lincoln, B. J., Lenn, Y. D., Green, J. A. M., Sundfjord, A., & Bacon, S. (2015). Tide-mediated warming of Arctic halocline by Atlantic heat fluxes over rough topography. *Nature Geoscience*, *8*, 191–194. https://doi.org/10.1038/ngeo2350

Rudels, B. (2015). Arctic Ocean circulation, processes and water masses: A description of observations and ideas with focus on the period prior to the International Polar Year 2007–2009. *Progress in Oceanography*, *132*, 22–67. https://doi.org/10.1016/j.pocean.2013.11.006

Rudels, B., Jones, E. P., Schauer, U., & Eriksson, P. (2004). Atlantic sources of the Arctic Ocean surface and halocline waters. *Polar Research*, *23*(2), 181–208. https://doi.org/10.1111/j.1751-8369.2004.tb00007.x

Rudels, B., Meyer, R., Fahrbach, E., Ivanov, V. V., Østerhus, S., Quadfasel, D., et al. (2000). Water mass distribution in Fram Strait and over the Yermak Plateau in summer 1997. *Annales Geophysicae*, *18*(6), 687–705. https://doi.org/10.1007/s00585-000-0687-5

Savel'eva, N. I., Semiletov, I. P., & Pipko, I. I. (2008). Impact of synoptic processes and river discharge on the thermohaline structure in the East Siberian Sea shelf. *Russian Meteorology and Hydrology*, *33*(4), 240–246. https://doi.org/10.3103/S1068373908040079

Schlosser, P., Newton, R., Ekwurzel, B., Khatiwala, S., Mortlock, R., & Fairbanks, R. (2002). Decrease of river runoff in the upper waters of the Eurasian Basin, Arctic Ocean, between 1991 and 1996: Evidence from $\delta^{18}O$ data. *Geophysical Research Letters*, *29*(9), 1–3. https://doi.org/10.1029/2001GL013135

Shimada, K., Carmack, E. C., Hatakeyama, K., & Takizawa, T. (2001). Varieties of shallow temperature maximum waters in the Western Canadian Basin of the Arctic Ocean. *Geophysical Research Letters*, *28*(18), 3441–3444. https://doi.org/10.1029/2001GL013168

Shimada, K., Itoh, M., Nishino, S., McLaughlin, F., Carmack, E., & Proshutinsky, A. (2005). Halocline structure in the Canada Basin of the Arctic Ocean. *Geophysical Research Letters*, *32*(3). https://doi.org/10.1029/2004GL021358

Shroyer, E. L., & Pickart, R. S. (2018). Pathways, timing, and evolution of Pacific winter water through Barrow Canyon. Deep Sea Research Part II. *Topical Studies in Oceanography*. https://doi.org/10.1016/j.dsr2.2018.05.004

Steele, M., & Boyd, T. (1998). Retreat of the cold halocline layer in the Arctic Ocean. *Journal of Geophysical Research*, *103*(C5), 10419–10435. https://doi.org/10.1029/98JC00580

Steele, M., Morison, J., Ermold, W., Rigor, I., Ortmeyer, M., & Shimada, K. (2004). Circulation of summer Pacific halocline water in the Arctic Ocean. *Journal of Geophysical Research*, *109*. https://doi.org/10.1029/2003JC002009

Timmermans, M. L., Proshutinsky, A., Golubeva, E., Jackson, J. M., Krishfield, R., McCall, M., et al. (2014). Mechanisms of Pacific summer water variability in the Arctic's Central Canada Basin. *Journal of Geophysical Research: Oceans*, *119*(11), 7523–7548. https://doi.org/10.1002/2014JC010273

Timokhov, L. A. (1994). Regional characteristics of the Laptev and the East Siberian Seas: Climate, topography, ice phases, thermohaline regime, circulation. In H. Kassens, H. W. Hubberten, S. M. Pryamikov, & R. Stein (Eds.), *Russian-German cooperation in the Siberian Shelf seas: Geo-system Laptev Sea* (Vol. 144, pp. 15–31). Ber. Polarforsch.

Tschudi, M., Meier, W. N., Stewart, J. S., Fowler, C., & Maslanik, J. (2019). *Polar Pathfinder Daily 25 km EASE-Grid Sea Ice Motion Vectors, Version 4. [Indicate subset used]*. NASA National Snow and Ice Data Center Distributed Active Archive Center. https://doi.org/10.5067/INAWUWO7QH7B

Weingartner, T. J., Danielson, S., Sasaki, Y., Pavlov, V., & Kulakov, M. (1999). The Siberian Coastal Current: A wind- and buoyancy-forced Arctic coastal current. *Journal of Geophysical Research*, *104*(C12), 29697–29713. https://doi.org/10.1029/1999JC900161

Williams, W. J., & Carmack, E. C. (2015). The 'interior' shelves of the Arctic Ocean: Physical oceanographic setting, climatology and effects of sea-ice retreat on cross-shelf exchange. *Progress in Oceanography*, *139*, 24–41. https://doi.org/10.1016/j.pocean.2015.07.008

Woodgate, R. A., Aagaard, K., Swift, J. H., Falkner, K. K., & Smethie, W. M., Jr. (2005). Pacific ventilation of the Arctic Ocean's lower halocline by upwelling and diapycnal mixing over the continental margin. *Geophysical Research Letters*, *32*(18). https://doi.org/10.1029/2005GL023999

Yamagami, A., Matsueda, M., & Tanaka, H. L. (2017). Extreme Arctic cyclone in August 2016. *Atmospheric Science Letters*, *18*(7), 307–314. https://doi.org/10.1002/asl.757

Zhao, J., Wang, W., Kang, S., Yang, E., & Kim, T. (2015). Optical properties in waters around the Mendeleev Ridge related to the physical features of water masses. *Deep Sea Research Part II: Topical Studies in Oceanography*, *120*, 43–51. https://doi.org/10.1016/j.dsr2.2015.04.011

Zhong, W., Zhang, J., Steele, M., Zhao, J., & Wang, T. (2019). Episodic extrema of surface stress energy input to the Western Arctic Ocean contributed to step changes of freshwater content in the Beaufort Gyre. *Geophysical Research Letters*, *46*(21), 12173–12182. https://doi.org/10.1029/2019GL084652